

RESEARCH PAPER

Structural and Optical Properties of Palladium , Silver, Core-Shell Nanoparticles Prepared using Pla Technique for Antibacterial Activation

Sajjad A. Hussain *, Mushtaq Talib Al-Helaly

Department of Physics, college of Education, University of Al-Qadisiyah, Iraq

ARTICLE INFO

Article History:

Received 15 March 2025

Accepted 26 May 2025

Published 01 July 2025

Keywords:

Core-Shell Nanoparticles

Laser ablation

Nd-YAG Laser

Palladium

Silver

ABSTRACT

In this research, (Pd-Ag core-shell nanoparticles) was prepared using (PLA) technique with (Nd-YAG) laser at a wavelength of 532nm, a power of (1J) and a number of different laser pulses. The structural properties (Pd-Ag core-shell Nps) were studied. The average physical size of the nanoparticles was obtained through (XRD and SEM) examination, and it increased with the increase in the number of laser pulses. The EDX examination showed that the prepared samples were of high purity. The results of optical properties tests showed an increase in absorbance and absorption coefficient and a decrease in transmittance with increasing number of laser pulses.

How to cite this article

Hussain S., Al-Helaly M. Structural and Optical Properties of Palladium , Silver, Core-Shell Nanoparticles Prepared using Pla Technique for Antibacterial Activation . J Nanostruct, 2025; 15(3):847-862. DOI: 10.22052/JNS.2025.03.004

INTRODUCTION

The process of Laser ablation to generate nanoparticles in liquids is a widely used process at the present time, although some of the resulting particles are not clearly known, such as the concentration of particles and their size distribution, and studies are continuing in this regard [1].

The process of laser ablation in a liquid has many applications [2]. It can be entered in the electronic industries and biotechnology, and most importantly the production of nanoparticles for many metals such as (gold-silver-palladium-lead-copper) and others [3]. The laser ablation mechanism is generally when the laser beam is absorbed by the surface of the target (used metal) that is immersed in a liquid such as (deionized

* Corresponding Author Email: llsajadll94@gmail.com

water-ethanol-acetone) and others [4], taking into account the laser parameters of wavelength, energy, number of laser pulses, frequency, amount of liquid and its height For the metal piece that is removed after that, the surface of the material is melted or it evaporates and nanoparticles are generated [5], and by changing the laser parameters mentioned, the size and concentration of the resulting particles can be controlled [6]

Metal nanoparticles are used in a wide range of applications as they are used in biomedicine due to their small size and selectivity for bacteria, as well as their anti-disease activity as they have a non-specific microbial toxicity mechanism [7,8].

The nanoparticles resulting from laser ablation of metal alloys in a liquid have many interesting properties that can be used in technology and



This work is licensed under the Creative Commons Attribution 4.0 International License.

To view a copy of this license, visit <http://creativecommons.org/licenses/by/4.0/>.

scientific research and lies in their use in sensing and stimulation systems, energy conversion and storage and in the field of Nano medicine [9].

MATERIALS AND METHODS

(pd-Ag core-shell Nps) were prepared using (PLA) technique by (Nd-YAG) laser with a wavelength of (532nm) in (10mL) deionized water with different number of laser pulses as shown in the Fig. 1 and Table 1.

Then the structural properties were studied (XRD, SEM, EDX). The nanoparticles were diluted on glass bases at room temperature, as shown in the Fig. 2.

RESULTS AND DISCUSSION

XRD (X-ray diffraction)

examinations of the [Pd-Ag core-shell NPS]

samples shown in Fig. 3 showed that the intensity increased slightly with increasing the number of laser pulses and that the D rate calculated from the Spark equation increased with increasing the number of laser pulses [9], as in the Table 2.

The purpose of measuring X-ray diffraction of nanoparticles is to know the crystalline nature of these particles and determine their crystal size. This examination also reveals the pattern of cubic structures. The basic information of the peaks that appeared in the laboratory results of (XRD) for all prepared samples was analyzed and the (Origin Pro 8) program was used to draw and give the final results. As we notice in Fig. 1 which shows the X-ray diffraction measurements of palladium and silver nanoparticles (Pd-Ag) NPs that Fabricated by pulsed laser ablation in deionized water (PLAL) using the second harmonic of the wavelength (532



Fig. 1. The pulsed Nd-YAG laser system used in the work.

Table 1. Show the Number of Laser Pulses for Each Sample.

Sample	Number of laser pulses
S1A	Pd 500
	Ag 250
S2A	Pd 750
	Ag 350
S3A	Pd 1000
	Ag 500
S4A	Pd 1250
	Ag 675

nm) and with different pulse numbers (250@500 pulse) and When using laser energy (500mJ) notice the appearance of two distinct peaks at (39.6, 46.2 = θ 2) respectively and they have the

highest intensity at Miller coefficients (*) (°) respectively and according to what is mentioned in the numbered card (JCPDS NO. 01-087-0638) Ag: (JCPDS card No. 04-0783) at issued by (Joint

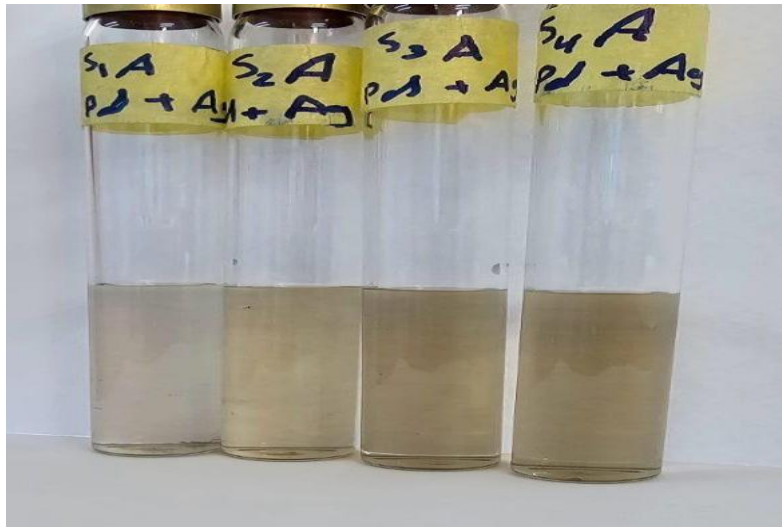


Fig. 2. shows a Photography image of the prepared samples.

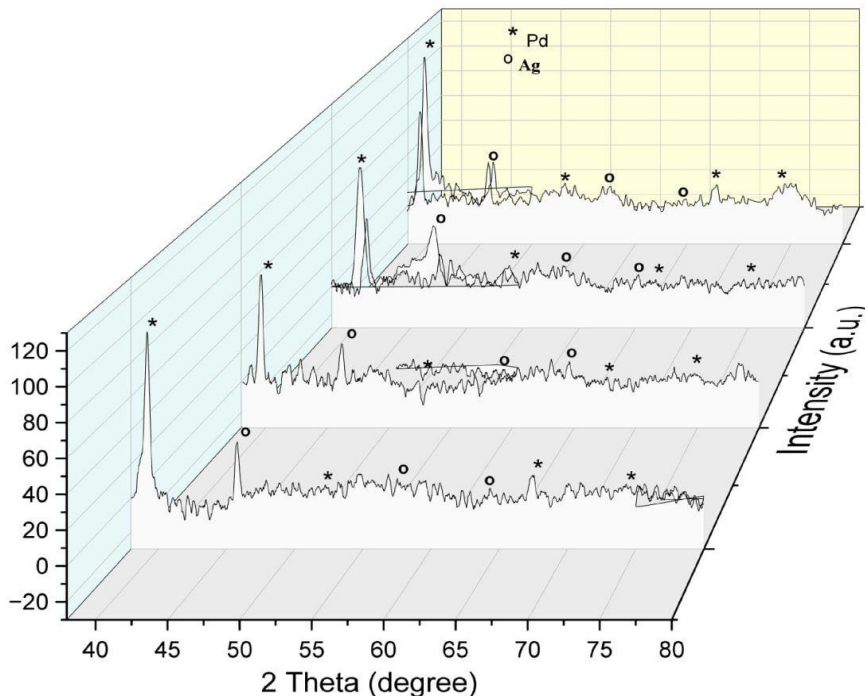


Fig. 3. (XRD) peaks using the wavelength (532 nm).

committee on powder diffraction standards [10], which is the joint committee on the standard diffraction card for powder materials. Through the drawing, we can also notice the appearance of a third peak but it is less intense than the previous two peaks. It appears at $(73.1 = \theta_2)$ and has the highest intensity at Miller coefficients (*) according to the above-mentioned card. Under the same previous working conditions, a laser energy of (500 mJ) and a number of pulses (350@750 pulse) were used. X-ray diffraction measurements were observed for palladium and silver nanoparticles Produced by laser ablation in deionized water. We also notice the appearance of two distinct peaks at and) $40.6, 41.7 = \theta_2)$ respectively, which have the highest intensity at Miller coefficients ($^{\circ}$) (*) respectively. A third peak was also observed, but it was less intense than the previous two peaks and its shape was irregular and random at $(75.9 = \theta_2)$ and has the highest intensity at Miller coefficients (*). The crystal size was also calculated for all these values using the (Scherer) equation. From this, we can conclude that the X-ray diffraction intensity is high when we used a laser energy of (500 mJ) for a wavelength of (532 nm). In addition, the crystal size was calculated (Crystal size) for these

peaks appearing using the (Scherer) equation as shown in Table 1 which shows the values of the crystalline levels and the average grain size of the palladium and silver nanoparticles as well

as the maximum width at the middle of the peak (FWHM) and the distance between the levels (d-spacing). As for the laser energy (500mJ) for the same wavelength (532nm) and the number of pulses (pulse500@1000) that were prepared under the same previous working conditions, we find that the analysis of the X-ray diffraction data for these nanoparticles also shows two prominent peaks at) $39.5^{\circ} 45.7, = \theta_2)$ respectively, and they have the highest intensity at Miller coefficients ($^{\circ}$) (*) respectively. In addition, a third peak appears that is less intense than the previous two peaks at $(74.4 = \theta_2)$ and has the highest intensity at Miller coefficients (*). As for the laser energy (500mJ) the same wavelength (532nm) and the number of pulses (1250@675 pulse) that were prepared under the same previous working conditions, we find that the analysis of the X-ray diffraction data for these nanoparticles also shows two prominent peaks at $(39.7, 45.9 = \theta_2)$ respectively, which have an intensity at Miller coefficients ($^{\circ}$) (*) respectively. In addition, a third value appears that is less intense than the previous two peaks at $(75.06 = \theta_2)$ and has the highest intensity at Miller coefficients (*).

Also, as shown in Table 2, we find that the solution that was prepared is characterized by high purity. Looking at the average particle size of the particles, we find that there is a difference between the sizes from energy to and the number

Table 2. shows the crystal size value and average particle size of the resulting palladium and silver nanoparticles when using a wavelength of (532 nm).

Films No.	Mixture Type and Pules No.	2 θ (deg)	θ (deg)	d (nm)	cos(θ)	FWHM (β) rad	(D) nm
S1A	Pd@Ag 500@250	39.6	19.8	0.227513658	0.940940099	0.008630017	17.06827296
		46.2	23.1	0.196430386	0.919901668	0.007924433	19.01313082
		73.1	36.55	0.129404718	0.803530023	0.095770681	1.801061523
S2A	Pd@Ag 750@350	40.6	20.3	0.222137512	0.937951235	0.008284468	17.83685826
		41.7	20.85	0.216528334	0.934581077	0.010668412	13.90101376
		75.9	37.95	0.125311376	0.788754174	0.108503141	1.619493645
S3A	Pd@Ag 100@500	39.5	19.75	0.228066583	0.941235052	0.706904014	0.208307396
		45.7	22.85	0.198462593	0.921603121	0.000139092	1081.223793
		74.4	37.2	0.127462015	0.796728878	0.014397906	12.08240378
S4A	Pd@Ag 1250@675	39.7	19.85	0.226963579	0.94064443	0.000191972	767.5376339
		45.9	22.95	0.197644234	0.920924641	0.000191972	783.9729417
		75.06	37.53	0.126504038	0.793236729	0.049804887	3.508233246

of other different pulses, as we notice that the more pulses used in the ablation process, the smaller the particle size, and this indicates the quality of the production of nanoparticles by the laser ablation process in a liquid when using a different laser and number of pulse [11].

The size of the crystals of these particles was calculated using the Debye-Scherrer equation, Eq. 1 [12]:

$$D = (0.94 \lambda) / (\beta \cos \theta) \quad (1)$$

D = particle size, K = phase constant, λ = wavelength, β = FWHM,

θ = Braak angle

By observing the peaks that appear in the (XRD) analysis, we find that these peaks are sharp and clear, which indicates that the resulting palladium and silver (Pd-Ag) NPs nanoparticles are well crystallized and can be polycrystalline.

The distance between crystal planes (d-spacing) was also calculated by Bragg's diffraction law, Eq. 2, and these values show good comparison with the standard values for palladium and silver

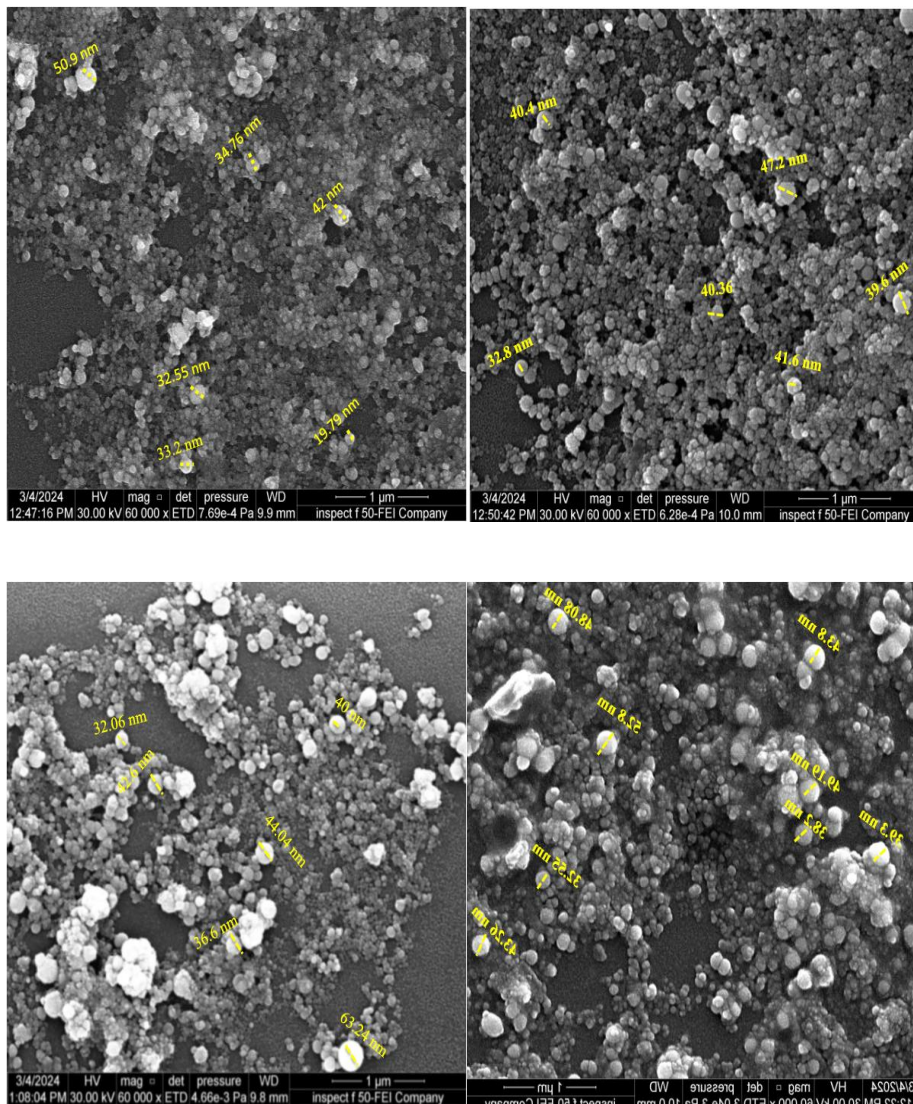


Fig. 4. Pd@Ag nucleus shell (532 nm) in water.

nanoparticles [12].

$$2d_{hkl}\sin\theta = n\lambda \quad (2)$$

d is the distance between crystal planes, θ is the angle of incidence of X-rays, n is an integer representing the order of interference.

It was also found that palladium and silver nanoparticles have cubic crystal phase and also the high range of peaks appearing indicates an increase in crystal size.

This result is consistent with the standard results. In addition, this increase in crystal structure can be interpreted as an enhancement of film crystallization by reducing crystal defects, i.e. crystals grow in one direction. In conclusion, all

the results presented above are good and almost consistent with the standard results [13].

Scanning Electron Microscopy (SEM)

Samples for SEM experiments were prepared by depositing a drop of solution containing Pd@Ag nanoparticles on silicon grids and leaving them to dry completely at room temperature. The liquid medium has a significant effect on the structure of PLAL nanoparticles. SEM images of Pd@Ag nanoparticles produced by the PLAL process in two distinct surrounding liquids (polymer and distilled water) are shown in Fig. 4. The nanoparticles are spherical or almost spherical, as shown in the SEM images in the figures. The SEM images in the figures also show that there are many spherical core-shell nanoparticles in liquids, especially in liquid

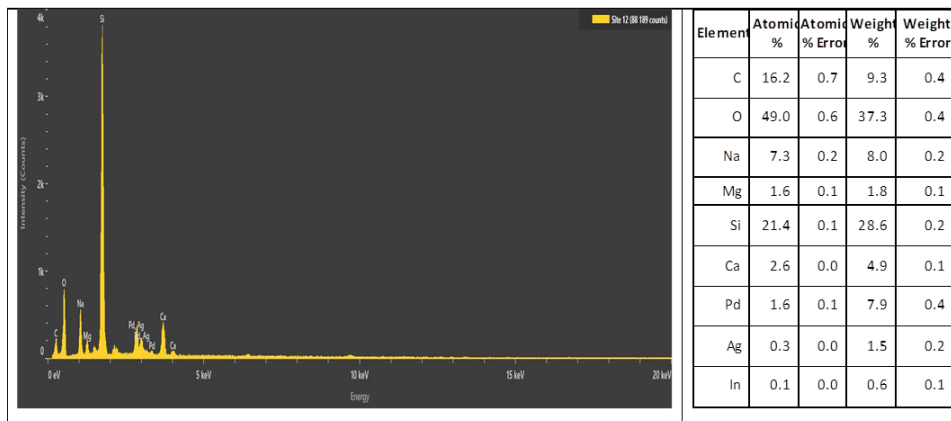


Fig. 5. Edx plot of palladium-silver (Pd-Ag)NPs nanoparticles produced by laser ablation at a wavelength of (532 nm).

Table 3. shows the particle sizes of the samples.

Films No	Mixture Type and Pules No.	Particle Grain size(nm)
S1A	Pd@Ag 500@250	35.53
S2A	Pd@Ag 750@350	40.32
S3A	Pd@Ag 100@500	43.09
S4A	Pd@Ag 1250@675	49.59

environments (compared to other environments). The results reveal that the average size and size distribution of nanoparticles in a given liquid environment vary. The optical properties of the target materials, such as absorption coefficient, and their physical properties, such as thermal conductivity, melting and boiling temperatures, electron-phonon coupling constant, and surface energy, contribute to this variation. These target characteristics were found to affect distinct stages of nanoparticle evolution.

Compared to ablation at lower wavelengths, nanoparticles generated at higher wavelengths have larger particle size [14,15] .

The number of different ablation energy pulses increases with decreasing laser wavelength. Laser atomization in liquids (LFL) results in smaller particle size, which reduces the number of energy pulses required for ablation despite higher ablation at shorter wavelengths.

This figure also observes agglomeration and clustering of the samples.

Increasing the laser flux leads to the formation of small droplets of palladium and silver which fragment as a result of their interaction with the incident laser beam, followed by rapid quenching, thus forming larger nanoparticles. When the laser flux is increased with increasing wavelength, pure hexagonal nanoparticles are observed as shown in the figures, which is in good agreement with the

XRD results [16].

Increasing the laser flux rate results in the formation of larger hexagonal particles and some rod-like structures. The effect of laser flux rate on the morphology of palladium-silver and palladium-silver nanoparticles can be explained based on the properties of the plasma generated on the surface target. The van der Waals attraction potential increases with increasing laser flux rate, leading to an increase in the density of agglomerated and clustered particles. Irregular particles were observed when the laser wavelength was increased to 532 nm. This result can be explained on the basis that increasing the laser flux

rate results in an increase in pressure and temperature, which in turn collapses the cavitation bubbles and thus gives irregular shaped particles [12].

Energy dispersive spectroscopy (EDS)

The test confirmed the chemical properties of colloidal solutions of metallic palladium and silver prepared in a laboratory using laser ablation in deionized water. had high purity for some samples, but other samples contained some impurities that were probably generated during the precipitation process., Different ratios of elements like (oxygen-carbon-sodium-magnesium) were observed but not taken into account. The Fig. 5 proves the presence of palladium and silver by plotting the

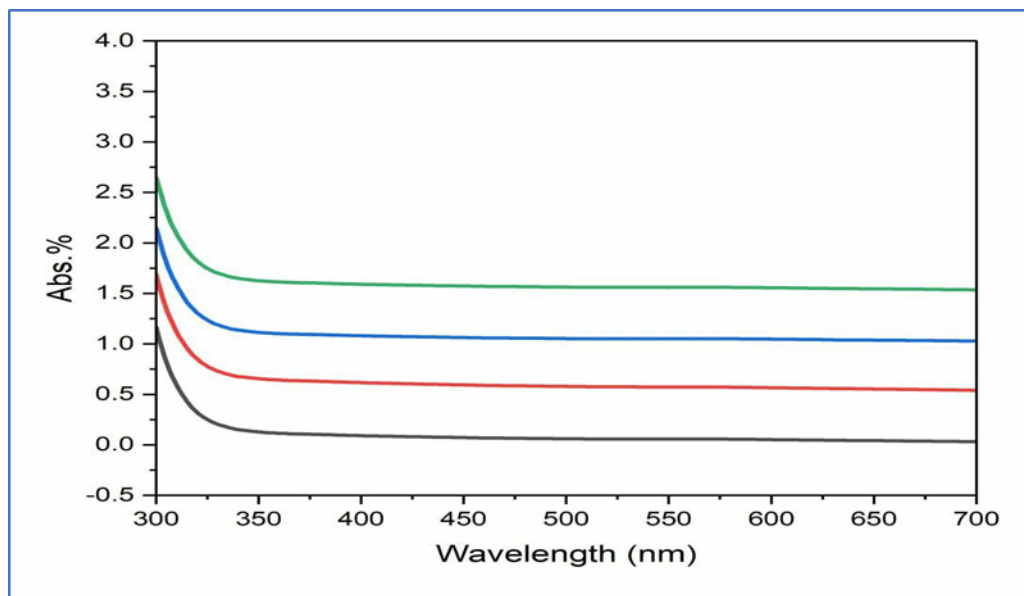


Fig. 6. Optical absorption spectrum of (Pd-Ag)NPs using the second.

positions The first signal was observed in the Edx spectrum point profiles. reflects palladium and silver, the second signal reflects oxygen, and the rest reflect atoms of other elements. [17].

The edx test results indicate that all samples, including palladium and silver, remained unchanged during preparation, as indicated by the intensity of the fall and the energy of the incident electron.

Optical linear properties

Absorbance

Fig. 6 shows the absorbance (Pd-Ag core-shell nanoparticont). We note from the figure that with the increase in the number of laser pulses, the absorbance increased due to the increase in the density of the generated nanoparticles and thus the increase in interactions between photons and nanoparticles, which led to an increase in the absorbance [18].

$$A = \frac{I_A}{I^0} \tag{3}$$

Coefficient of Absorption

Fig. 7 shows the absorption coefficient and we notice an increase in the absorption coefficient with the increase in the number of laser pulses. The same reason that led to the increase in absorbance is because the absorption coefficient is directly proportional to the absorbance according to the relationship [14].

$$\alpha = 2.303 \frac{A}{t} \tag{4}$$

Transmittance

Permeability. Fig. 8 shows the permeability and we notice a decrease in permeability with the

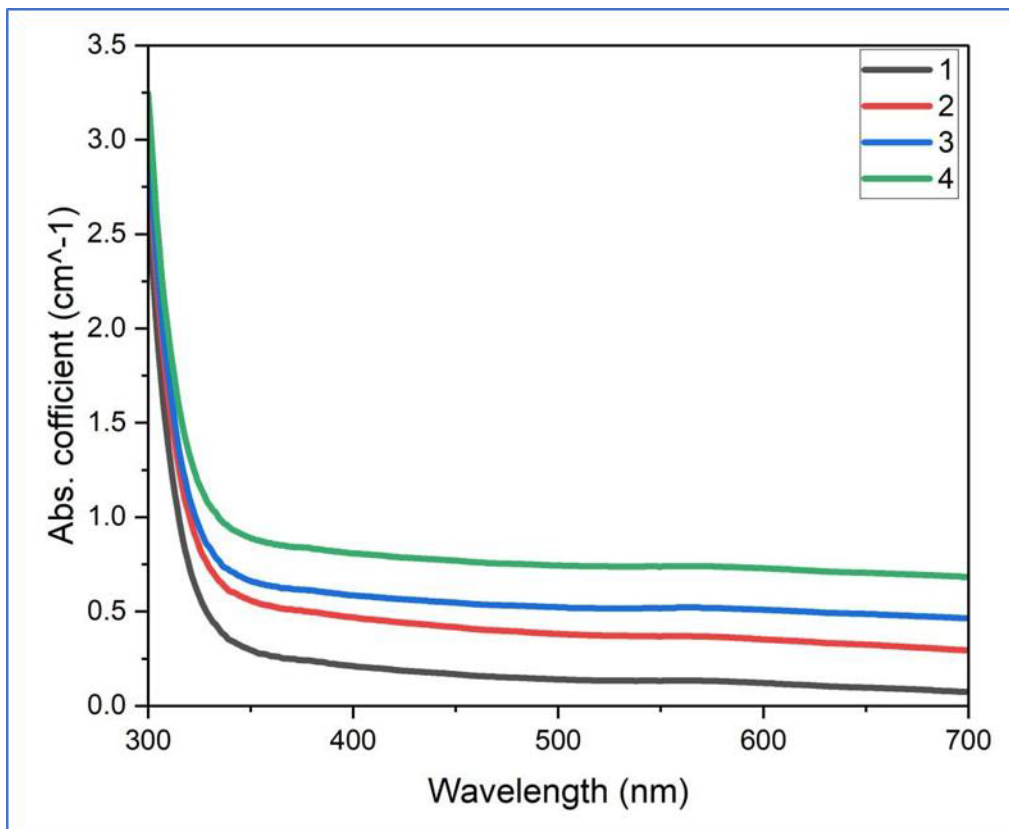


Fig. 7. Absorption coefficient spectrum of (Pd - Ag)NPs when using the second harmonic of the wavelength.

increase in the number of laser pulses. The same reason that led to the decrease in permeability is because permeability is inversely proportional to absorbance according to the following relationship [15]:

$$T = \frac{1}{A} \quad (5)$$

Antibacterial efficacy of palladium and silver nanoparticle solutions

After testing Laser ablation prepared palladium silver colloid solution on two Common bacteria, such as Staphylococcus aureus and Escherichia coli,

as seen in Figs. 9 and 10, which display distinct inhibition zones on the Mueller Hinton agar surface that contain both. Analysis of the When the colloidal solutions were given to bacteria, it was demonstrated that they could inhibit the growth of “Escherichia coli” and “Staphylococcus aureus.”

Comparing the effects of palladium and silver nanoparticle solutions prepared using one wavelength (532 nm), we found that the greater the number of strokes used, the larger the inhibition zone diameters for Gram-negative

bacteria (Escherichia coli) and Gram-positive bacteria (Staphylococcus aureus), as shown in Table 4.

We found similar inhibition values for both Gram-positive (Staphylococcus aureus) and Gram-negative (Escherichia coli) bacteria. This implies that palladium’s antibacterial action is what caused the bacterial reaction. and there are no notable differences between these two kinds of bacteria in terms of silver nanoparticles. The inhibitory zone is formed in part by the bacterial cell wall. The Gram-positive bacterial cell wall (S. aureus) consists of a deep layer of a membrane The nanoparticles consist of linear polysaccharide chains, but in Gram-negative bacteria (Escherichia coli), their wall consists of a thin film layer. This suggests that the nanoparticles have a large enough surface area to interact with each other, thereby enhancing the antibacterial effect.

Different inhibition values for different pulse numbers when producing palladium and silver nanoparticles have completely opposite effects on bacteria. It can be concluded that using different pulse both Gram-negative (Escherichia coli) and Gram-positive (Staphylococcus aureus) bacteria. This suggests that the bacterial response was brought on by palladium’s antibacterial properties.

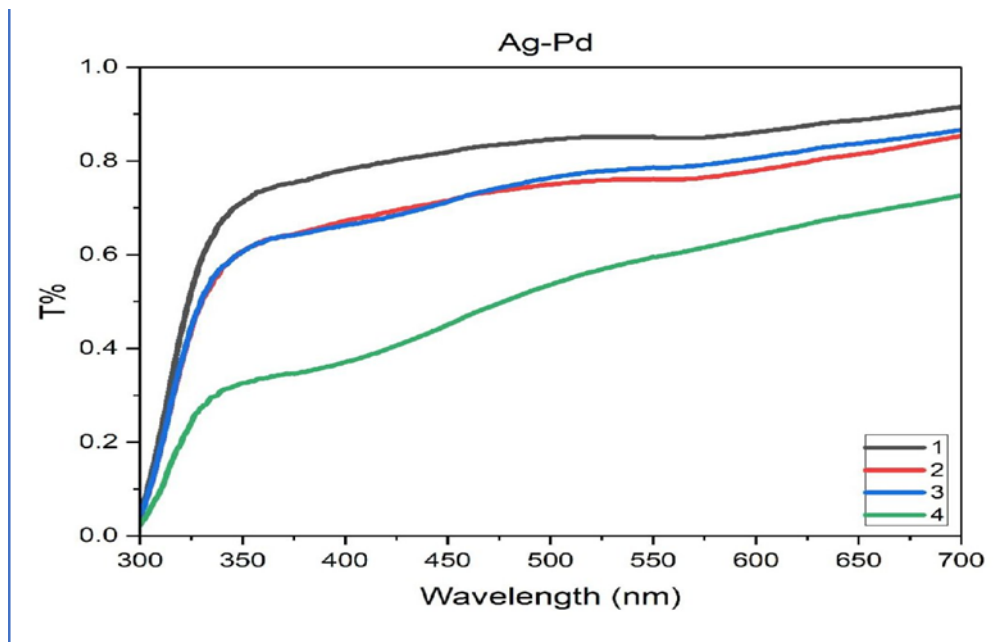


Fig. 8. Represents the transmittance spectrum of (Pd - Ag)NPs using the second harmonic of the wavelength.

... the silver nanoparticle content of these two types of bacteria does not significantly differ from one another. The bacterial cell wall contributes to the formation of the inhibitory zone. The Gram

The inhibition value is very high compared to other metal nanoparticles. This confirms the

superiority of palladium and silver nanoparticles in antibacterial activity [16].

Effective → (5 mm – 10 mm)

Good effect → (10 mm-20 mm)

High efficiency → (20 mm and above)

The inhibitory impact of the palladium and

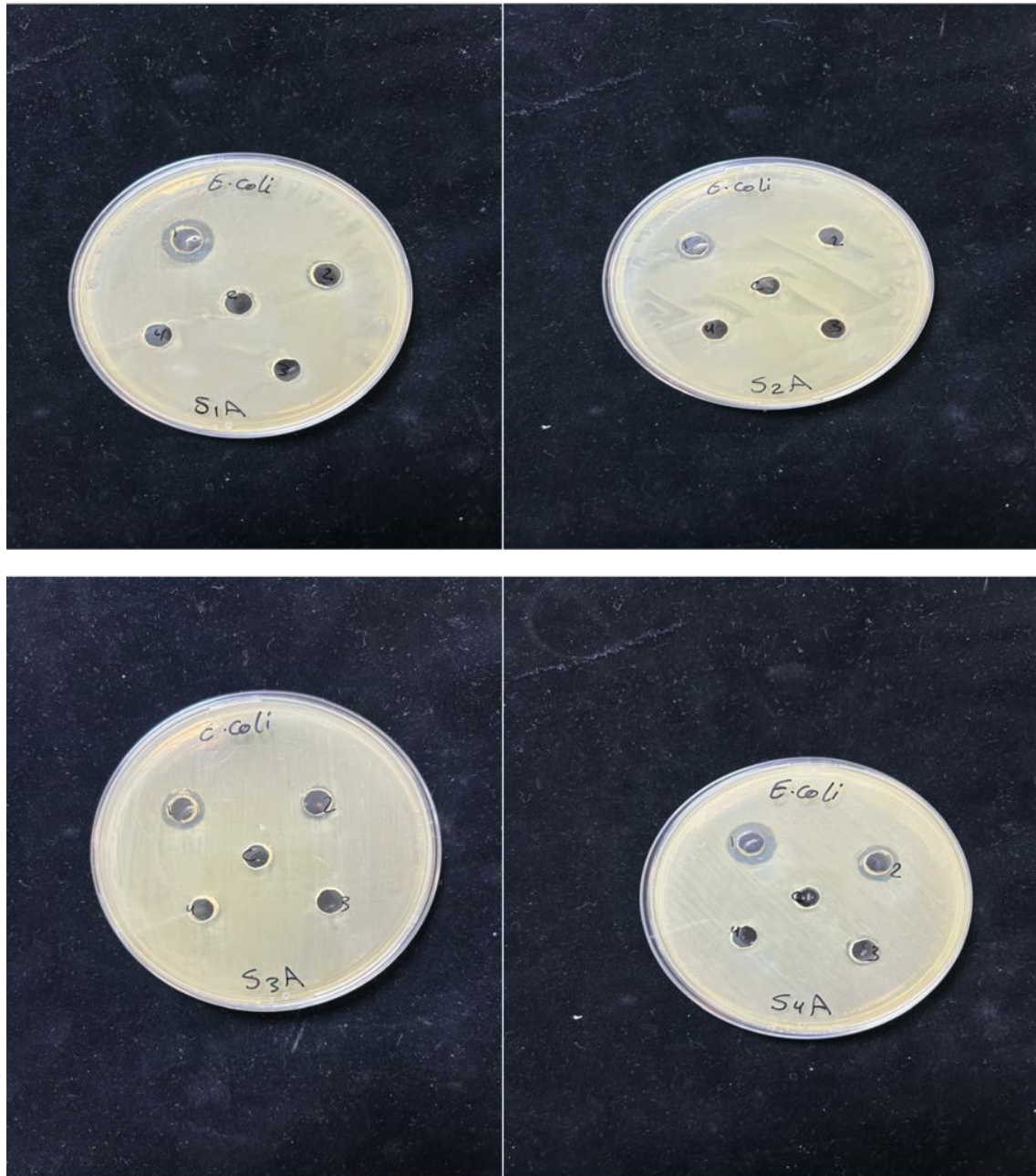


Fig. 9. Shows inhibition area of Escherichia coli was observed using palladium and silver nanoparticles at varying wavelengths and pulse numbers through laser ablation in deionized water.

silver nanoparticle sizes on the two employed microorganisms is evident as the surface area of these particles has a greater antimicrobial effect compared to their small diameter. These

particles are rich in reactive oxygen species (ROS), including (OH), (H₂O₂), and (O₂⁻) which, when penetrated and infiltrated the bacterial cell wall, lead to high reactivity, causing significant damage

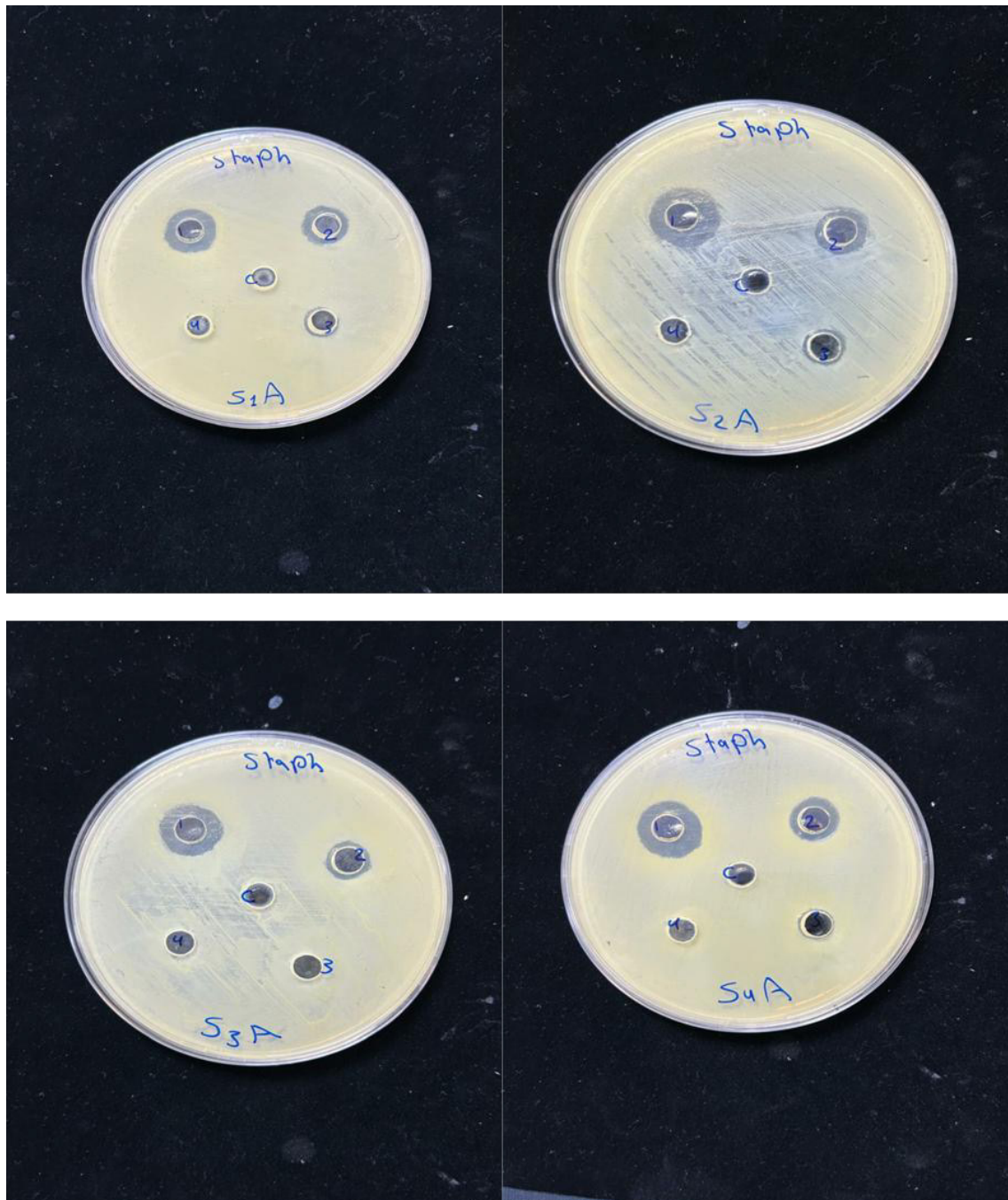


Fig. 10. shows images of the inhibition zone of the bacteria "Staphylococcus aureus" produced by laser ablation in deionized water at different wavelengths and pulse numbers using palladium and silver nanoparticles.

to the proteins and DNA of the bacterial cells, thus destroying the cell membrane, allowing its contents to seep out. They have the ability to enter the microbial cells from within, and when adhered to the cell membrane, interact with the cell structure and important components such as enzymes, lipids and DNA, thus reducing the respiration of the bacterial cells, thus destroying

and killing them.

Studies have shown that Both Gram-positive (*Staphylococcus aureus*) and Gram-negative (*Escherichia coli*) bacteria are highly sensitive to antibiotics and have poor resistance. solutions of palladium and silver nanoparticles. We discovered by merely looking at the inhibition zone that the highest inhibition

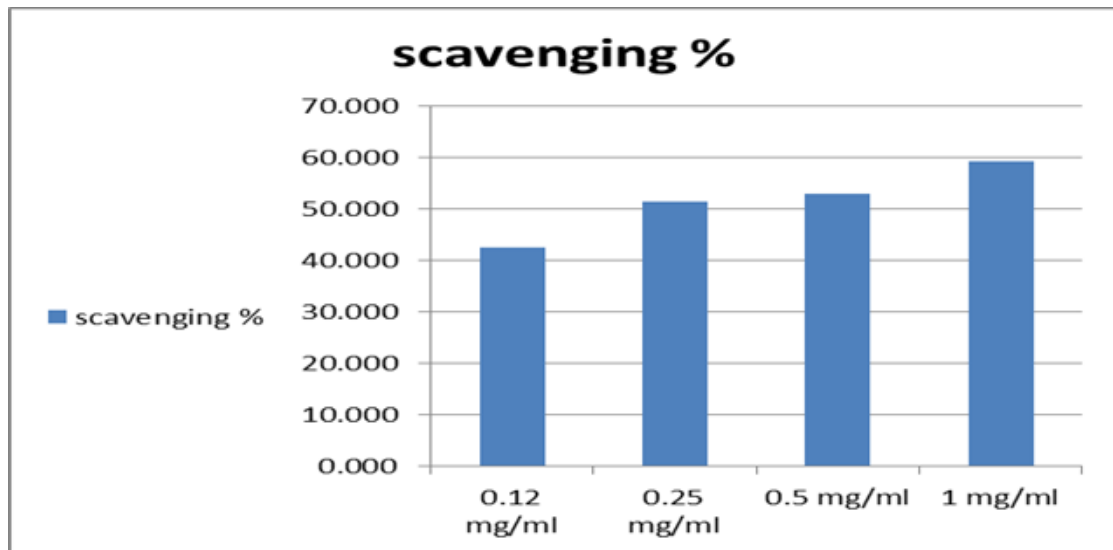


Fig. 11. Antioxidant effect of palladium and silver nanoparticles synthesized in DPPH test.

Table 4. Inhibition rates for the two types of bacteria (*E. coli*) and (*S. aureus*) using the second harmonic of the wavelength

NO.	Number of laser pulses	G -negative (<i>E. coli</i>)	G -positive (<i>S.aureus</i>)
1	Pd 500	10	15
2	Ag 250	0	11
3		0	9
4		0	0
1	Pd 750	12	14
2	Ag 350	9	11
3		0	0
4		0	0
1	Pd 1000	14	16
2	Ag 500	12	12
3		9	10
4		0	0
1	Pd 1250	15	13
2	Ag 675	11	11
3		0	8
4		0	0

effect was the sample with a wavelength of 532 nm prepared with different pulse numbers and energy (500 mJ). The inhibition effect was 10 μ m for E. coli and 10 μ m for S. aureus. bacteria is (15 mm). The second sample comes immediately after

it with an inhibition amount for (E.coli) bacteria (12 mm) and for (S. aureus) bacteria (14 mm), where these samples have shown good effectiveness. The diameter of inhibition for the bacteria is at which the third sample was prepared, the

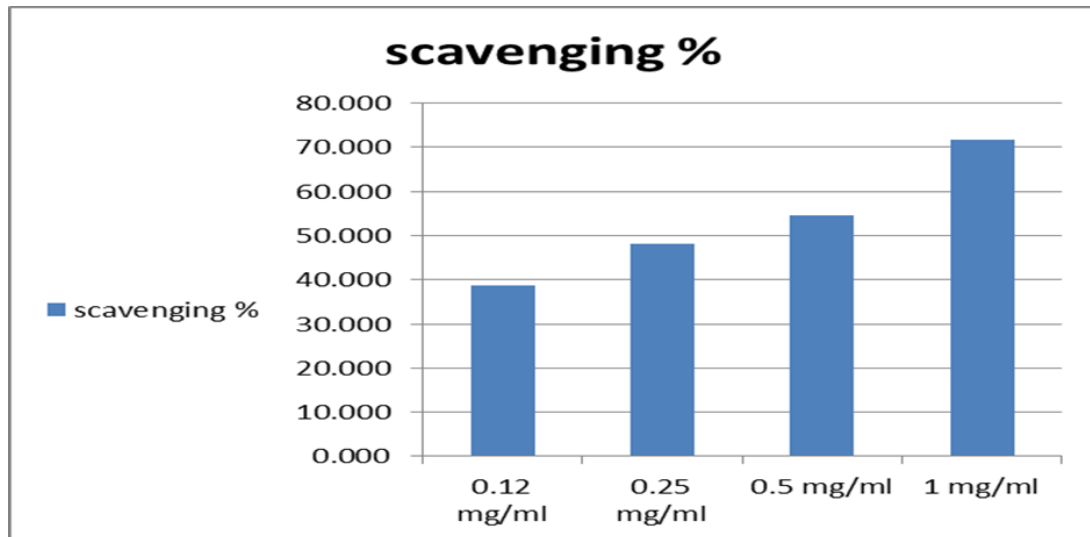


Fig. 12. Antioxidant effect of palladium and silver nanoparticles synthesized in DPPH test.

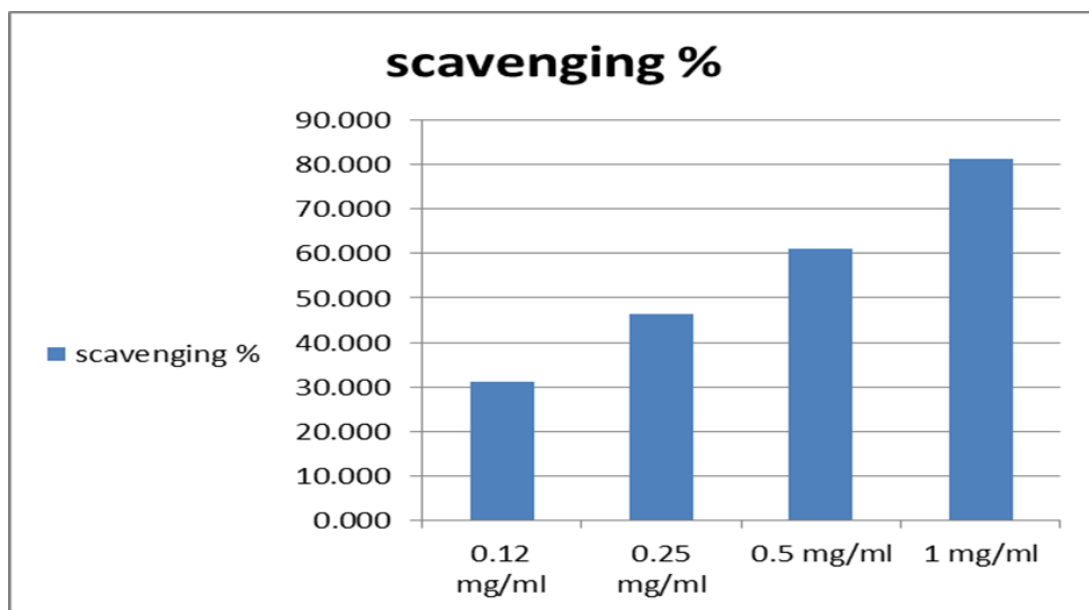


Fig. 13. Antioxidant effect of palladium and silver nanoparticles synthesized in DPPH test.

inhibition amount for (E.coli) bacteria is (14 mm) and for (S.aureus) bacteria is (16 mm). The fourth sample was prepared with an inhibition amount for (E.coli) bacteria (15 mm) and for (S.aureus) bacteria (13 mm).

We conclude from the above that palladium-silver nanoparticle (Pd-Ag)NPs solution has high antibacterial efficacy against both microorganisms that are both Gram-positive and Gram-negative. This trait can be found in samples. with different energy values and pulse numbers due to increasing palladium concentrations. and silver nanoparticles. However, we observed a higher bacterial growth inhibition rate in samples with a higher pulse number. This is due to the small particle size of the nanoparticles, which allows them to penetrate the cell wall quickly and easily. Another reason is the presence The primary cause of bacterial mortality and destruction is reactive oxygen species (ROS). [17].

Both Gram-negative (Escherichia coli) and Gram-positive (Staphylococcus aureus) bacteria demonstrated minimal resistance and high susceptibility to colloidal palladium solution. with Escherichia coli showing a stronger response to the antibacterial effect of palladium and silver nanoparticles than S. aureus.

Antioxidant activity of Pd-Ag NPs nanoparticles

The effect of palladium and silver nanoparticles

prepared using the pulsed laser ablation method in distilled water at a wavelength of 532 nm(and a different pulse frequency, using a laser energy of 500 mJ(. DPPH (1-Diphenyl- 2-picrylhydrazyl). A free radical scavenging experiment was conducted to determine the antioxidant capacity of palladium and silver nanoparticles in vitro by reducing DPPH free radicals. Thirty minutes after introducing nanoparticles at concentrations of) 0.12, 0.25, 0.5, and 1 µg/ml(to the DPPH solution, the absorbance at 517 nm was determined. The ability of the nanoparticles to scavenge DPPH free radicals was demonstrated by measuring color changes [18]. DPPH, which reduces the effect of nanoparticles, increased with increasing concentrations of bioactive palladium and silver nanoparticles.

It was 59.3% at 1 µg/ml, 52.9% at 0.5 µg/ml, 51.5% at 0.25 µg/ml, and 42.5% at 0.12 µg/ml for palladium and silver nanoparticles, as shown in Fig. 11.

1-Diphenyl-2-picrylhydrazyl, which reduces the activity of the nanoparticles, increases with increasing concentration of palladium and silver bio-nanoparticles. 7.71% at 1 µg/ml, 54.5% at 0.5 µg/ml, 48.1% at 0.25 µg/ml, and 38.6% at 0.12 µg/ml palladium and silver nanoparticles, as shown in Fig. 12.

1- Diphenyl-2-picrylhydrazyl, which reduces the activity of the nanoparticles, increases with increasing concentration of palladium and silver

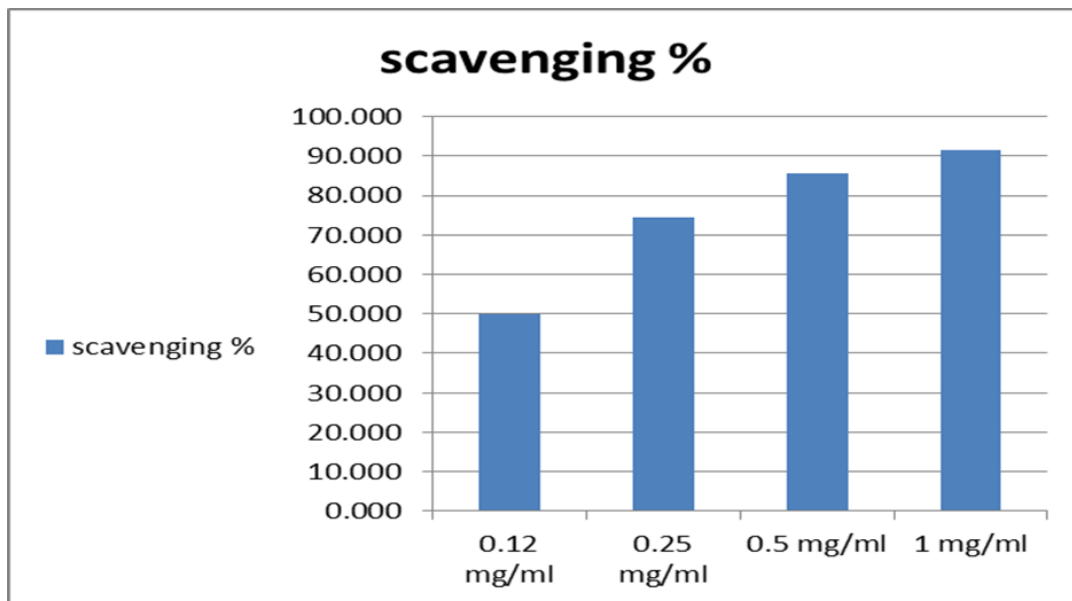


Fig. 14. Antioxidant effect of palladium and silver nanoparticles synthesized in DPPH test.

bio-nanoparticles: 81.4% at 1 $\mu\text{g/ml}$, 61.1% at 0.5 $\mu\text{g/ml}$, 46.4% at 0.25 $\mu\text{g/ml}$, and 31.0% at 0.12 $\mu\text{g/ml}$ palladium and silver nanoparticles, as shown in Fig. 13.

Diphenyl-2-picrylhydrazyl, which reduces the activity of the nanoparticles, increases with increasing concentration of palladium and silver bio-nanoparticles. 91.4% at 1 $\mu\text{g/ml}$, 85.6% at 0.5 $\mu\text{g/ml}$, 74.5% at 0.25 $\mu\text{g/ml}$, and 49.9% at 0.12 $\mu\text{g/ml}$ palladium and silver nanoparticles, as shown in Fig. 14.

A single compound, 1-diphenyl-2-picrylhydrazyl (DPPH), has been commonly used to assess the antioxidant free radical scavenging capabilities in vitro. DPPH appears to be a more stable and well-known free radical that relies on the reduction of palladium and silver nanoparticles. By observing the color change, the antioxidant potential of DPPH was tested. The DPPH scavenging activity of the nanoparticles increased with increasing concentration, indicating that the inhibition ratio of DPPH increased with increasing concentration of palladium and silver nanoparticles, suggesting that DPPH exhibited greater inhibition due to increased donation in the nanoparticles. Antioxidants function not only by scavenging free

radicals but also by inhibiting the formation of free radicals [19].

Free radicals have a powerful bactericidal effect on oxidative stress. Not only was the membrane damaged, but major biological molecules such as proteins, lipids, DNA enzymes, and DNA that promote cell death also caused damage [20].

Effect of palladium and silver nanoparticles on hemolysis

Hemolysis is a condition in which red blood cells rupture and release their components, leading to anemia, jaundice, and kidney failure. Because all substances entering the blood come into contact with red blood cells, it is crucial to assess the hemolytic potential of the substances [21].

Hemolysis was determined using Triton X-100 as a positive control. Sterile phosphate-buffered saline was used as a negative control, allowing the base solution to be stored at room temperature. Palladium and silver NPS particles at all concentrations (1, 0.5, 0.25, and 12 $\mu\text{g/ml}$) did not induce hemolysis in the whole blood samples examined, as shown in Table 5, and . This finding is consistent with [22], who found that hemolysis is not caused by the nanoparticles or the solvents

Table 5. Effect of palladium and silver nanoparticles on hemolysis

Sample	Haemolysis %
Triton X-100 (positive control)	100
PBS(negative control)	0
Blood with Pd@AgNPs 0.12 $\mu\text{g/ml}$	0
Blood with Pd@AgNPs 0.25 $\mu\text{g/ml}$	0
Blood with Pd@AgNPs 0.5 $\mu\text{g/ml}$	0
Blood with Pd@AgPs 1 $\mu\text{g/ml}$	0

present in the nanoparticles or polymer.

CONCLUSION

Palladium silver (Pd-Ag) NPs nanoparticles were prepared using the laser-in-liquid (LI) technique. The liquid used was deionized water (DIW). A wavelength of 532 nm, an energy of 500 mJ, and a different pulse count were used for each sample. Tests were performed on the samples obtained, including UV-Vis testing, to determine the absorbance, absorptivity, and transmittance of the Pd-Ag nanoparticles. It was observed that the absorbance value and the absorption coefficient of the nanoparticles varied with the number of pulses. the more laser pulses that are used to create the Pd-Ag) NPs, the higher the absorbance and absorption coefficient values, and the lower the transmittance value. XRD and SEM tests were performed. Scanning electron microscope (SEM) analysis showed the that resulting particles are spherical in shape and aggregate to form various shapes and cubic crystalline structures of the Pd-Ag nanoparticles. (Edx) to ascertain the chemical makeup and purity of the samples utilized in biological testing. Palladium-silver nanoparticles' efficacy as colloidal solutions was onfirmed as antibacterial, antioxidant, and hemolytic, whether negative or positive. We also concluded The palladium sample with the highest inhibition was found to be the one with a wavelength of 532 nm. for bacteria (*Escherichia coli*).

CONFLICT OF INTEREST

The authors declare that there is no conflict of interests regarding the publication of this manuscript.

REFERENCES

- Dudoitis V, Ulevičius V, Račiukaitis G, Špirkauskaitė N, Plauškaitė K. Generation of metal nanoparticles by laser ablation. *Lithuanian Journal of Physics*. 2011;51(3):248-259.
- Sánchez-López E, Esteruelas G, Ortiz A, Espina M, Prat J, Muñoz M, et al. Dexibuprofen Biodegradable Nanoparticles: One Step Closer towards a Better Ocular Interaction Study. *Nanomaterials* (Basel, Switzerland). 2020;10(4):720.
- Scaramuzza S, Agnoli S, Amendola V. Metastable alloy nanoparticles, metal-oxide nanocrescents and nanoshells generated by laser ablation in liquid solution: influence of the chemical environment on structure and composition. *Physical Chemistry Chemical Physics*. 2015;17(42):28076-28087.
- Chen C, Gao Y, Jiang J, Han J. Wavelength-Dependent Nonlinear Absorption in Platinum Nanoparticles at Off-Resonant Wavelength. *Photonics*. 2022;9(8):545.
- Fadhil N, Jasim F. Study of optical and structural properties of prepared gold nanoparticles by pulse laser ablation method. *Journal of Education and Science*. 2021;30(4):69-82.
- Monodisperse Thioether-Stabilized Palladium Nanoparticles: Synthesis, Characterization, and Reactivity. American Chemical Society (ACS).
- Mahdi MA, Khadayeir AA, Dahash IB, Shaheed MA. Structural properties of Zn doped CuO thin film by DC magnetron sputtered. *AIP Conference Proceedings: AIP Publishing*; 2023. p. 070033.
- Azara Hussain S, Jabbar Radi A. Study the effect of film thickness on the structural and optical of (ZnO) thin film prepared by pulsed laser deposition. *Journal of Physics: Conference Series*. 2019;1294(2):022001.
- Kumar BR, Rao TS. Structural and optical properties of DC reactive magnetron sputtered zinc aluminum oxide thin films. *AIP Conference Proceedings: AIP Publishing LLC*; 2014. p. 118-122.
- Fouad OA, Makhlof SA, Ali GAM, El-Sayed AY. Cobalt/silica nanocomposite via thermal calcination-reduction of gel precursors. *Materials Chemistry and Physics*. 2011;128(1-2):70-76.
- Tang C-W, Wang C-B, Chien S-H. Characterization of cobalt oxides studied by FT-IR, Raman, TPR and TG-MS. *Thermochim Acta*. 2008;473(1-2):68-73.
- Oneizah LHA, Kareem QS, Shaheed MA. Investigation of the non-linear optical characteristics of gold nanoparticles doped with distilled water (DDDW) by laser. *AIP Conference Proceedings: AIP Publishing*; 2025. p. 040022.
- Su J-F, Huang Z, Yuan X-Y, Wang X-Y, Li M. Structure and properties of carboxymethyl cellulose/soy protein isolate blend edible films crosslinked by Maillard reactions. *Carbohydr Polym*. 2010;79(1):145-153.
- Rashid SN, et al. Effect of CO2 Laser Irradiation on the Topographic and Optical Properties of CdO Thin Films. *Baghdad Science Journal*. 2020;17(1(Suppl.)):0318.
- Hussain SA, Radi AJ, Najim FA, Shaheed MA. Structural, Optical and Sensing Properties of ZnO:Cu Films Prepared by Pulsed Laser Deposition. *Journal of Physics: Conference Series*. 2020;1591(1):012088.
- Prisinda D. Antibacterial Potential Test of Basil Leaf (*Ocimum Basilicum*) Against *Enterococcus Faecalis* ATCC 29212. *International Journal Of Medical Science And Clinical Research Studies*. 2021;01(04).
- Gold K, Slay B, Knackstedt M, Gaharwar AK. Antimicrobial Activity of Metal and Metal-Oxide Based Nanoparticles. *Advanced Therapeutics*. 2018;1(3).
- Podder S, Chanda D, Mukhopadhyay AK, De A, Das B, Samanta A, et al. Effect of Morphology and Concentration on Crossover between Antioxidant and Pro-oxidant Activity of MgO Nanostructures. *Inorganic Chemistry*. 2018;57(20):12727-12739.
- Huang T, Holden JA, Heath DE, O'Brien-Simpson NM, O'Connor AJ. Engineering highly effective antimicrobial selenium nanoparticles through control of particle size. *Nanoscale*. 2019;11(31):14937-14951.
- Sienicki K. Comment on the Paper Titled 'The Origin of Quantum Mechanical Statistics: Insights from Research on Human Language' (arXiv preprint arXiv:2407.14924, 2024). *MDPI AG*; 2024. <http://dx.doi.org/10.20944/preprints202411.2377.v1>
- Swain P, Das R, Das A, Padhi SK, Das KC, Mishra SS. Effects of dietary zinc oxide and selenium nanoparticles on growth performance, immune responses and enzyme activity in rohu, *Labeo rohita* (Hamilton). *Aquacult Nutr*. 2018;25(2):486-494.
- Baravkar PN, Sayyed AA, Rahane CS, Chate GP, Wavhale RD, Pratinidhi SA, et al. Nanoparticle Properties Modulate Their Effect on the Human Blood Functions. *BioNanoScience*. 2021;11(3):816-824.